Arrays of magnetic nanodots on nitrogen-modified Cu(001) surfaces

2002 J. Phys.: Condens. Matter 14 8177

(http://iopscience.iop.org/0953-8984/14/35/302)

INSTITUTE OF PHYSICS PUBLISHING JOURNAL OF PHYSICS: CONDENSED MATTER

J. Phys.: Condens. Matter **14** (2002) 8177–8197 PII: S0953-8984(02)33592-6

Arrays of magnetic nanodots on nitrogen-modified Cu(001) surfaces

F Komori, S Ohno and K Nakatsuji

Institute for Solid State Physics, University of Tokyo, Kashiwa-shi, Chiba 277-8581, Japan

Received 8 February 2002, in final form 27 May 2002
Published 22 August 2002
Online at stacks.iop.org/JPhysCM/14/8177

Abstract

A self-organized nanometre-scale pattern on a nitrogen-adsorbed Cu(001)-c(2 × 2) surface is used as a template for the fabrication of a magnetic nanodot array. By adjusting the coverage of nitrogen on this surface, 5 nm × 5 nm square patches of the c(2 × 2)–N surface can be arranged squarely and separated by 2 nm wide strips of clean Cu surface. Magnetic transition metals grow selectively on the clean Cu surface, and two-monolayers thick dots are dominantly formed at the intersections of the 2 nm wide Cu strips. Consequently, magnetic dots of a few nanometres in diameter are squarely organized with 7 nm intervals. Both the formation of the nitrogen-adsorbed nanopattern and the growth of the magnetic nanodots have been studied in detail by using scanning tunnelling microscopy and electron diffraction. Strain relief of the partly nitrogen-covered surface is the driving force producing the square arrangement of the nitrogen-adsorbed patches. The organization of the magnetic dots is ascribed both to selective nucleation of the magnetic metal dots on the clean Cu surface and to the large growth rate at the intersections. The magneto-optical Kerr effect is employed to examine the magnetic properties of the Co dot array. A long-range order among double-layer dots is established before their percolation occurs with increasing size. The origin of the novel magnetism is discussed.

1. Introduction

Both the progress in vacuum technology and the accumulated knowledge in surface science have allowed us to study well-characterized magnetic thin films and nanostructures on clean surfaces in ultrahigh vacuum (UHV). Various kinds of magnetic transition and rare-earth metal have been used to prepare them so far, and their magnetic properties have been investigated *in situ* in UHV. Magnetic nanostructures on solid substrates are stable, and thus suitable not only for providing qualitative knowledge on nanometre-scale magnetism, but also widely in industrial applications. In addition, they show promise as regards fabrication of new magnetic materials by controlling the nanostructure and the combination of elements. At present, the

study of magnetic nanostructures on solid surfaces is focused both on the formation mechanism and on the origin of the magnetism. On the other hand, in view of one of their potential applications, much effort has been made to realize ultrahigh-density magnetic recording by using assemblies of nanometre-scale ferromagnets.

Small particles of ferromagnetic metals have been studied for over 50 years. The important findings at the early stages were the appearance of single magnetic domains and superparamagnetism. In the 1960s, physical properties of small metallic particles a few tens of nanometres in diameter started to be intensively investigated using samples prepared by the method of evaporation into an inert gas. Large amounts of round-shaped particles are routinely produced by this method although the particles are weakly connected by naturally grown oxide on the surface. Small magnetic particles with similar size have also been made by various other methods such as chemical reduction and spark erosion. Experimental studies using these samples clearly showed single-domain remanent magnetization at low temperature, and their thermally activated rotations—that is, superparamagnetism—while quantitative analyses were difficult because of their uncharacterized surfaces and interconnections. We had to await the development of the experimental technique in UHV to overcome the difficulties, in the middle of the 1980s. The study of ultrathin magnetic films has undergone especially great development in the decades since then [1, 2]. The wide variety of recent studies on magnetic thin films and nanostructures on clean surfaces in UHV have recently been reviewed by Himpsel *et al* [3]. The magnetism of the well-characterized individual particles has been studied by using cluster beams in UHV combined with Stern–Gerlach measurements [4]. In this article, we concentrate on the ensembles of magnetic nanoparticles at surfaces, especially the regular arrangement on a nitrogen-adsorbed Cu(001) surface.

2. Magnetic nanostructure at surfaces

Thin ferromagnetic transition metals on normal-metal substrates have been intensively studied in efforts to achieve an understanding of low-dimensional magnetism. In these systems, magnetic long-range order is established by increasing the nominal thickness of the transition metals within a few atomic monolayers (MLs). For example, for Fe(110)/W(110) [5], detailed measurements of the surface morphology and the magnetic transition revealed that the ordering process is a two-dimensional (2D) magnetic percolation. A similar mechanism for the long-range order was proposed for Co/Cu(001) [6].

The above two kinds of magnetic film grow in a layer-by-layer mode and the magnetic percolation takes place between the single layer and the double layer. On the other hand, Fe and Co three-dimensional (3D) islands are formed on Cu(111) surfaces at room temperature (RT). Cobalt islands with triple layers were observed before the percolation of the islands [7], and are surrounded by Cu brims. The observed magnetic moment of Fe on this surface was about 0.5 μ_B [8], which is smaller than that on the Cu(001) surface. Multi-layered 3D Co islands are also formed on Cu(110) surfaces, and there is no ferromagnetic response until the average Co thickness reaches 4.2 ML at RT [9]. The morphology, composition, and crystal structures of the magnetic metal overlayers, which affect the magnetism, are largely dependent on the substrate crystal orientations.

For the study of magnetic interaction in nanometre-scale structures, random networks of magnetic islands are not suitable for macroscopic measurements of spatially averaged quantities because of the inhomogeneities in the lateral size and the thickness of the magnetic islands. Moreover, in the case of usual 3D island growth, there is a certain relationship between the particle size and their separation. Thus, it is not easy to vary intentionally the parameters that determine the magnetic interactions among them. Controlled fabrication of

ordered nanometre-scale structures is required in order to study the size and shape dependence of the magnetic interaction.

One of the methods used to prepare regular nanostructures is selective step decorátion or step-flow growth of magnetic metals on a vicinal surface. We can utilize the thermodynamically stable steps on a clean surface as selective nucleation sites for magnetic metals. Isolated one-dimensional magnets form along step edges on adjusting the amounts of magnetic metal on vicinal surfaces and the growth temperature. Magnetic properties have been studied in iron stripes on vicinal W(110) [5, 10] and Cu(111) [11] surfaces. In the former case, the transition from an assembly of one-dimensional short magnets to a long-range 2D ferromagnetically ordered magnet was caused by the magnetic dipole interaction among the small magnets separated by non-magnetic terraces. In the latter, one-dimensional Ising behaviours were observed because of the negligibly small inter-chain interaction.

For the growth of ordered two-dimensional arrays of magnetic nanodots, self-organized strain-relief patterns on metal surfaces have been recently used as templates [12–16]. In particular, a number of structural studies have been made on a reconstructed Au(111) surface. Nickel [12] and cobalt [13] clusters are self-assembled at the elbows of the Au(111)-22 $\times \sqrt{3}$ herringbone reconstruction during the deposition at RT in UHV. The surface morphology has been studied in detail by using scanning tunnelling microscopy (STM). In the case of 1 ML Co deposition on average, these form round-shape dusters whose height is double atomic layers. At the initial stage of Ni deposition, selective exchange between the Ni atom and the substrate Au atom was found at the elbows of the herringbone structure in STM observations [17]. The substitutional atoms are considered to play the roles of nucleation centres for the growth of the small islands. It is noted that no selective island growth was found for Ag deposition on this surface [18], and the exchange is essential for the selective island growth of the magnetic metals.

Each isolated Co cluster on this surface shows superparamagnetism at RT [19, 20], and it is blocked at low temperature. On this surface, the distance between the particles perpendicular to the zigzag pattern is shorter than that along the pattern. This causes, at first, the one-dimensional magnetic coherence perpendicular to the zigzag pattern with increasing size of the double-layer Co dots at RT [20]. Further increase of the size induces a percolative transition to 2D long-range ferromagnetic order just like in the magnets on vicinal surfaces [10, 11].

We have been using an isotropic strain-relief pattern—that is, a nitrogen-modified Cu(001) surface. The surface structure of nitrogen-adsorbed Cu(001) is c(2 $\times$ 2) [21], and the saturation coverage is 0.5 ML. A novel ordered structure on this surface was first reported by Leibsle *et al* [22]. They showed that c(2 $\times$ 2)–N square patches about 5 nm $\times$ 5 nm in size can be arranged squarely separated by a few nanometres of clean Cu(001) surface by adjusting the amount of nitrogen and the annealing temperature. In other words, we can prepare a square grid of clean Cu(001) surface, each part a few nanometres wide, as schematically illustrated in figure 1(a). It has been considered [23] that this surface is formed to relieve the surface strain caused by the lattice mismatch between the Cu crystal and the c(2 $\times$ 2)–N patches.

Growth of magnetic [14, 15, 24–27] and non-magnetic [28] metals has been studied on this surface. These metals grow selectively on the clean Cu area of the surface at the early stage of the deposition at RT, although the detail of the growth is dependent on the metal species, the deposition rate, and the morphology of the surface. When the average thickness of the metal exceeds 1 ML, dots 2 ML thick are selectively formed at the lattice points of the Cu(001) grid as schematically illustrated in figure 1(b). Magnetic transition metals are known to grow pseudomorphically (fcc) with a certain distortion on a clean Cu(001) surface at least for several monolayers. The fcc Fe and fcc Co thin films on this surface are ferromagnetic, and details of the growth and the magnetism have been clarified [1–3]. Thus, truly 2D ferromagnetic dot arrays are formed on nitrogen-adsorbed Cu(001) by depositing Fe and Co on the grid patterns.

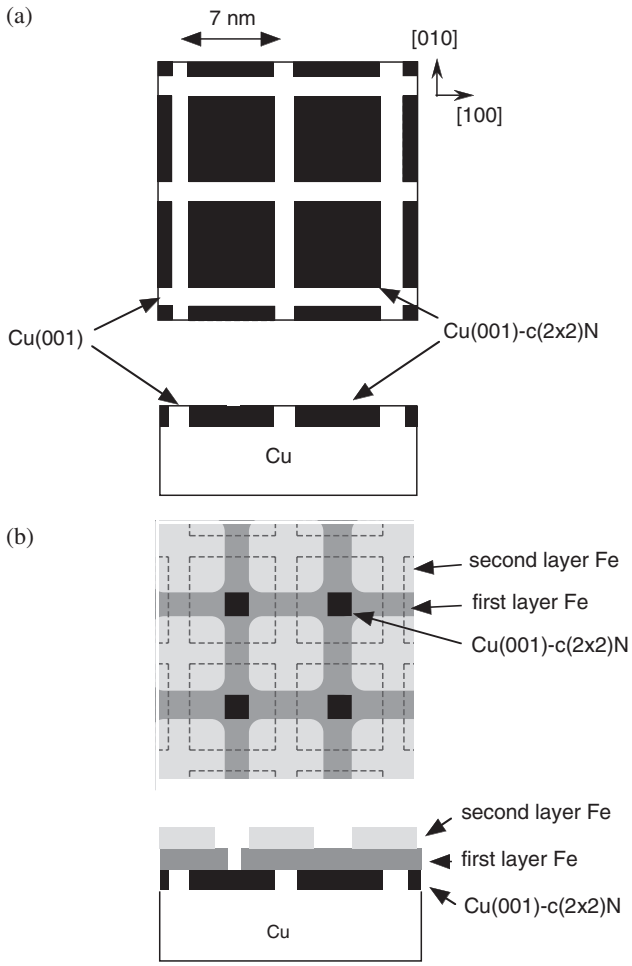

Figure 1. (a) A schematic illustration of the nitrogen-adsorbed Cu(001) surface where c(2 × 2)–N square patches are squarely arranged on a clean Cu surface. (b) A greyscale schematic illustration of the 2 ML thick magnetic dot array on the surface (a). Dashed lines indicate the boundaries between the c(2 × 2)–N patches and the clean Cu(001) surfaces.

We have studied in detail the growth of Fe and Co at RT using STM, and the magnetic properties of the Co dot array using the surface magneto-optical Kerr effect (SMOKE) [26, 29]. In this article, we will give detailed experimental results, and discuss the formation process of the dot arrays and their magnetic properties.

3. Experimental procedures

3.1. STM observation

Surface structures were observed using scanning tunnelling microscopes (DME, Rasterscope-3000 or Omicron, micro-STM) in two independent ultrahigh-vacuum systems, each of which consists of preparation and STM chambers. The latter is equipped with a four-grid low-energy electron diffraction (LEED) and Auger electron spectroscopy (AES) optics (BLD600, OCI),

and the former an Ar-ion gun. The base pressure for both chambers was better than 2×10^{-10} Torr. All STM images presented in this article were recorded in constant-current mode at RT using tungsten tips. The tunnelling current was 0.01–0.5 nA, and the sample bias voltage was between −3 and +3 V. The height of the STM image was calibrated using a monatomic step of Cu substrate.

A clean surface of Cu(001) was obtained by repeating Ar-ion sputtering (400–500 eV, 1 μA) for 15 min, and annealing at 670–1000 K in the preparation chambers. Then the cleaned sample was transferred to the STM chamber. We confirmed the cleanliness of the surface by AES, the structural order by finding a sharp 1×1 LEED pattern, and the surface morphology by STM.

To prepare the nitrogen-modified surface, the clean Cu(001) surface was bombarded by nitrogen ions of 400–500 eV, and then annealed at about 600 K for typically 5 min in the preparation chamber. We monitored the ion current at the sample during the nitrogen-ion bombardment to adjust the amount of nitrogen implanted into the substrate. The regular arrangement of c(2×2)–N square patches was confirmed by STM. At the same time, we monitored a satellite structure around the integral LEED spots [29–31]. To make a regular arrangement of the nitrogen-adsorbed patches, we have to adjust both the level of the ion dosage and the annealing conditions.

In the STM chambers, pure Co or Fe (99.999 %) was deposited on the nitrogen-modified surface from one of two sources: an alumina crucible, around which a resistively heated tantalum wire was wound; or the metal wire, directly heated by electron bombardment. We kept the substrate temperature at RT to reduce intermixing of the deposited metal and the Cu substrate [32]. The pressure during the deposition was less than 5×10^{-10} Torr. The deposition rate was monitored by a quartz microbalance, which was calibrated by the results of STM observations. It was between 0.1 and 2 ML min^{-1}. The averaged thickness of the deposited metal was estimated by measuring the total volume of the metal islands in the STM image. At the same time, we measured the intensity ratio of Co LMM(716 eV) or Fe LMM (703 eV) Auger lines to the Cu LMM(920 eV) line as a function of the averaged thickness of Co or Fe on the surface. In addition, the satellite structure around the integral LEED spots was monitored, and the periodic arrangement was confirmed.

3.2. Magnetization measurement

The magnetization curves were measured *in situ* using the SMOKE in another UHV system consisting of a measurement chamber with a LEED optics (OCI, BLD600) and a preparation chamber. The base pressures of the chambers were better than 2×10^{-10} Torr. The SMOKE signal was detected in longitudinal and polar configurations with s-polarized light from a He–Ne laser. Two pairs of Helmholtz coils for longitudinal and polar configurations were placed in the measurement chamber for this purpose. The coils were wound around Cu bobbins, which were in thermal contact with a liquid nitrogen reservoir. The fluence of the light was less than 1 mW mm^{-2}. A lock-in technique was employed by modulating the incident light with a photoelastic modulator. During the SMOKE measurement, the sample temperature could be controlled between 90 and 450 K. Temperature during the measurement was monitored by a thermocouple attached to the side of the Cu crystal.

The arrays of Co nanodots were prepared in the same way as for the STM experiments except that the Co source was either a resistively heated W wire wrapped with a Co wire or an electron-bombardment-type Co source. To ensure the substrate morphology with a regular arrangement of c(2×2)–N square patches, we utilized the LEED patterns showing the satellites around the integer-order spots. The thickness of Co was monitored by a quartz microbalance,

which was calibrated by the measured Co/Cu Auger ratio. Here we use the relation between the Co/Cu Auger ratio and the averaged Co thickness calibrated by the STM observation. To confirm the calibration of the deposition rate, we measured the Curie temperature (T_C) of Co films grown on clean Cu(001) surfaces as a function of the calibrated thickness. As in the literature [33], we defined T_C experimentally as the temperature at which the remanence magnetization detected by means of the SMOKE vanishes. We found that the values of T_C were consistent with those reported in this literature. The accuracy of the Co thickness obtained is about 15% because of the uncertainty in the measured Auger ratio.

4. Nitrogen-adsorbed Cu(001) surfaces

Figure 2 shows STM images of nitrogen-adsorbed Cu(001) surfaces. The nitrogen coverages are 0.1 ML (a), 0.2 ML (b), 0.3 ML (c), 0.4 ML (d), and 0.5 ML (saturation) (e) on average. When the amount of nitrogen at the surface is small, there are randomly distributed patches with the nitrogen-adsorbed c(2 × 2) structure on clean Cu(001) surfaces as in figure 2(a). The nitrogen-adsorbed surface is usually imaged lower than the clean Cu surface. With increasing amount of adsorbed nitrogen at the surface, the shape of the patches becomes square, and they arrange squarely, separated by lines of clean Cu(001) surface. The directions of the Cu lines are ⟨100⟩ as in figures 2(b), (c). When the surface is saturated by nitrogen, trenches along ⟨110⟩ directions appear with monatomic layer depth (figure 2(e)).

There are two typical patterns when both nitrogen-adsorbed area and clean Cu surface coexist. One is an anisotropic quasi-one-dimensional arrangement of clean Cu surface, where the width of the lines is anisotropic, as shown in figure 2(b). The other is a square grid pattern of clean Cu surface as shown in figure 2(c). These two kinds of arrangement were reported by Silva *et al* [25]. They claimed that the quasi-one-dimensional arrangement was realized by reducing the amount of nitrogen dosage. We obtained the former arrangement by increasing the annealing temperature to 620 K after the nitrogen-ion bombardment, keeping the other conditions the same. In this condition, both the diffusion and the desorption of nitrogen atoms are enhanced in comparison with the case for the annealing at 600 K. In one small domain of this surface, the width of bright Cu lines along the [100] direction is larger than that along the [010] direction, whereas we find the opposite in the other domain. This surface could be used as a possible template for the growth of one-dimensional magnets [25] although it is difficult to prepare a single-domain surface for macroscopic measurements.

Further increase of nitrogen coverage makes the width of the Cu lines narrower, and trench structures along the ⟨110⟩ direction coexist with squarely arranged nitrogen-adsorbed patches as shown in figure 2(d). The trench is one monolayer deep and 1–2 nm wide. On the nitrogen-saturated surface, the entire surface has the c(2 × 2)–N structure with a number of trenches, as in figure 2(e).

Even when the amount of nitrogen at the surface is very small, the size of the c(2 × 2)–N patches is limited. Ellmer *et al* [34] reported the formation process of the patches at 600 K. They observed separation of the patches during the nitrogen adsorption. When the size of the patch increases, two clean Cu lines along [100] and [010] are introduced to separate the patch into four small patches. This is believed to originate from the reduction of the interface strain between the patch and the substrate Cu crystal. The Cu lattice spacing at the nitrogen-adsorbed patch is different from that of the Cu crystal. Thus the strain due to this lattice mismatch at the interface between the patch and the Cu crystal underneath increase with increase in the size of the patch. Finally, the total strain energy becomes so large that the c(2 × 2)–N patch cannot expand further. Instead of that, clean Cu(001) lines are introduced at the centre of the large patches because the clean Cu surface is soft enough to relax the strain.

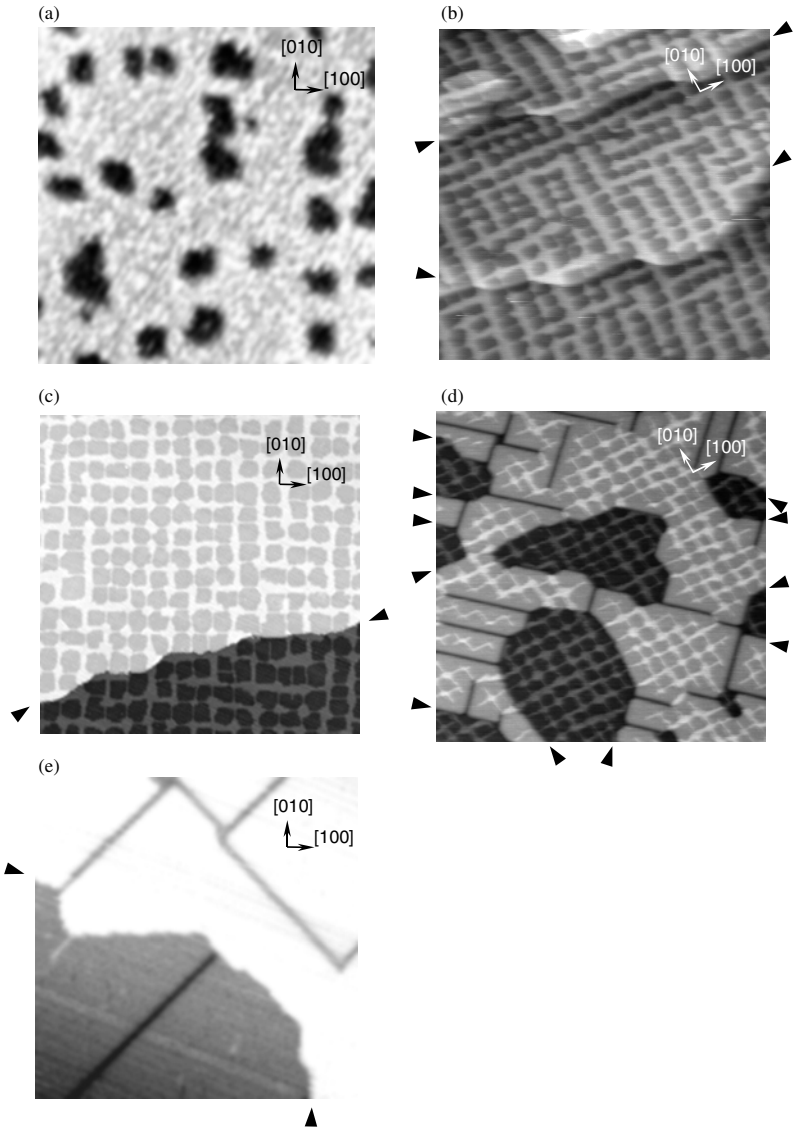

Figure 2. STM images of nitrogen-adsorbed surfaces prepared with five different conditions. Arrows indicate the positions of steps with the monatomic height. (a) The surface with c(2 × 2)–N patches (dark area) randomly distributing on clean Cu(001) surface (bright area). The nitrogen coverage of the surface is 0.1 ML on average. The image size is 40 nm × 40 nm. (b) The surface with anisotropic Cu lines. The nitrogen coverage of the surface is 0.2 ML on average. The image size is 125 nm × 125 nm. (c) The surface with squarely arranged c(2 × 2)–N patches (dark area) separated by clean Cu surface (bright square grids). The nitrogen coverage of the surface is 0.3 ML. The image size is 100 nm × 100 nm. (d) The surface with c(2 × 2)–N square patches and monatomic depth trenches. The density of Cu lines with subnanometre widths is higher than that shown in (c). The nitrogen coverage of the surface is 0.4 ML on average. The image size is 100 nm × 100 nm. (e) The nitrogen-saturated Cu(001) surface. Trenches are randomly distributed. The image size is 80 nm × 80 nm.

The strain-relief mechanism is also responsible for the regular array formation of the c(2 × 2)–N patches. The total strain energy can be minimized when the patches are

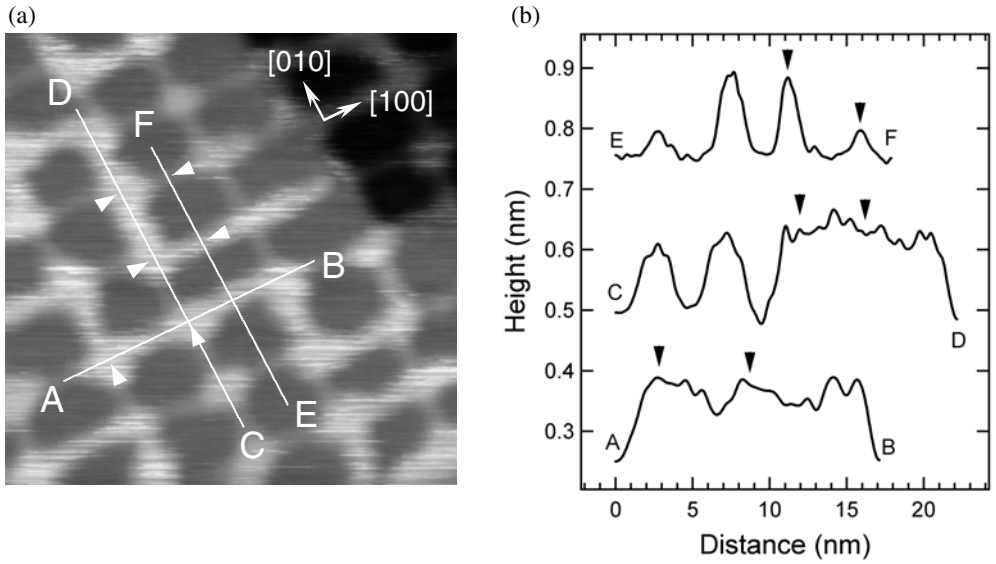

Figure 3. (a) An STM image of the surface consisting of Cu(001)-c(2 × 2)–N patches (dark square areas) and clean Cu(001) lines (bright lines). (b) Cross sections of the surface along the lines A–B, C–D, and E–F in (a). The solid triangles correspond to the positions shown as white triangles in (a).

regularly arranged. There remain, however, disorders in the width of the clean Cu lines and the shape of the patches, as we see in the STM images. The strain is inhomogeneously relieved during the annealing process. In spite of the local disorder, the macroscopically averaged period of the square grid is almost constant at 7 nm between 0.2 and 0.4 ML coverage of N, as observed by spot-profile LEED study [31].

Figure 3(a) shows a magnified STM image of the grid pattern, and figure 3(b) shows the cross sectional lines of the STM image along the lines A–B, C–D, and E–F in figure 3(a). The observed height of the clean Cu surface depends on the width of the line in this imaging condition. This is not an artefact due to the rapid scanning of the STM tip, because the height is independent of the scanning speed and the direction. The apparent height of the narrowest line in the figure is less than $1/4$ of those of the wider lines. We can even recognize that the height at the centre of the intersection is about 20% larger than at the middle of the 2 nm wide line (see A–B in figure 3(b)). The apparent height of the line is the same as that at the intersections for more than 3 nm wide lines, as shown by C–D of figure 3(b). These results indicate that the surface electronic state at the narrow Cu lines is different from those at the intersections. The change of the electronic states at the lines is ascribed both to the direct electronic effect of the nitrogen adsorption at the neighbouring c(2 × 2)–N patches and to the indirect effect of the strain of the Cu lattice due to the presence of the lattice-mismatched patches. For the 1 nm wide Cu lines, both the direct effect and the strain are large, and the apparent height is substantially reduced. On the other hand, for the Cu lines of more than 1 nm width, the direct electronic effect is weak because it only reaches the area within a distance equal to the screening length of the Cu crystal from the edges of the c(2 × 2)–N patches. Thus the observed variation in the electronic states between the wide Cu lines and the intersections is attributed to that of the surface strain.

The trenches on the nitrogen-adsorbed surfaces relieve the surface strain just like the grids of clean Cu lines. When the amount of surface nitrogen is increased, there remains little area

with clean Cu surface, and it is not enough to relieve the large surface strain. A monatomic step can also play the role of an area for strain relief, and the trench with two steps is introduced. We note that the density of the steps increases even after formation of the c(2 × 2)–N patches.

Very recently, the atomic structure of c(2 × 2)–N patches has been studied in detail using x-ray photoelectron diffraction [35] and STM [36]. On the basis of these observations, buckling of Cu atoms at the c(2 × 2)–N patches is proposed although this is not consistent with the previous observation [22] nor with a recent first-principles study [37]. The surface stress has also been studied by using He-ion channelling [38], and the result indicates large displacements of Cu atoms from the bulk crystal sites. The atomic structure and the detailed origin of the strain-relief pattern remain problems to be solved in future.

5. Two-dimensional arrangement of magnetic dots

5.1. Fe dot array

In figure 4, we show the STM images of iron-deposited Cu(001)-c(2 × 2)–N surfaces with clean Cu grid lines whose width is <3 nm. The average coverage of Fe is (a) 0.02 ML, (b) 0.05 ML, (c) 0.1 ML, (d) 0.9 ML, and (e) 1.4 ML. The deposition rate of Fe is 0.2 ML min^{-1}.

At the early stages of the deposition, monolayer Fe islands are selectively formed at the intersections of the clean Cu lines, and the density of the islands increases with increase in the average thickness of Fe up to 0.1 ML on average, as in figure 4. There are two kinds of selectivity as regards the growth. One is that between clean Cu surface and the c(2 × 2)–N surface. The other is the selection of the intersections of the lines among the clean Cu surfaces of the grid pattern. The former indicates that the diffusion barrier for the iron atoms at the c(2 × 2)–N surface is smaller than that at the clean Cu surface. Iron atoms freely migrate at RT on the nitrogen-adsorbed surface just after arrival, and move to clean Cu surface.

After most of the intersections are covered with 1 ML Fe, the monolayer islands grow laterally along the clean Cu lines and expand even over the c(2 × 2)–N patches from their edges with increasing amount of deposited Fe. Then most of monolayer islands are connected with one another, and finally double-layer islands start to grow at the centres of the intersections as shown in figures 4(d), (e). The morphology of this surface is schematically illustrated in figure 1(b) for figure 4(e), and the cross sections along the lines G–H and I–J in these figures are shown in figure 5. The observed height of the islands corresponds to double the Cu(001) atomic layer.

For all surfaces with averaged Fe coverage of up to 2 ML, the LEED patterns are always c(2 × 2) although the spots become dull with increasing Fe thickness. This indicates that the c(2 × 2)–N structure is stable against Fe deposition of a few ML, and that Fe growth is epitaxial on the substrate as in the case of Fe grown on clean Cu(001) at RT.

The distribution of the iron islands changes when we increase the deposition rate. The small islands are initially formed both on narrow Cu lines and the c(2 × 2)–N patches, as shown in figure 6(a). Here the deposition rate was 2 ML min^{-1}. This initial growth indicates that the nucleation occurs even on nitrogen-adsorbed patches during the migration process of Fe atoms on the patches owing to their increased density. When we deposit 0.03 ML Fe on average with the same rate, the large islands are selectively formed at the intersections of clean Cu lines, as shown in figure 6(b). The small islands nucleating initially on the Cu lines and the patches hardly grow any further during the additional deposition.

D'Addato *et al* [39] studied the structure of the same system by means of surface extended x-ray absorption fine structure (SEXAFS). The results suggested that the Fe islands have an fcc lattice structure with tetragonal distortion like Fe thin films on a clean Cu(001) surface.

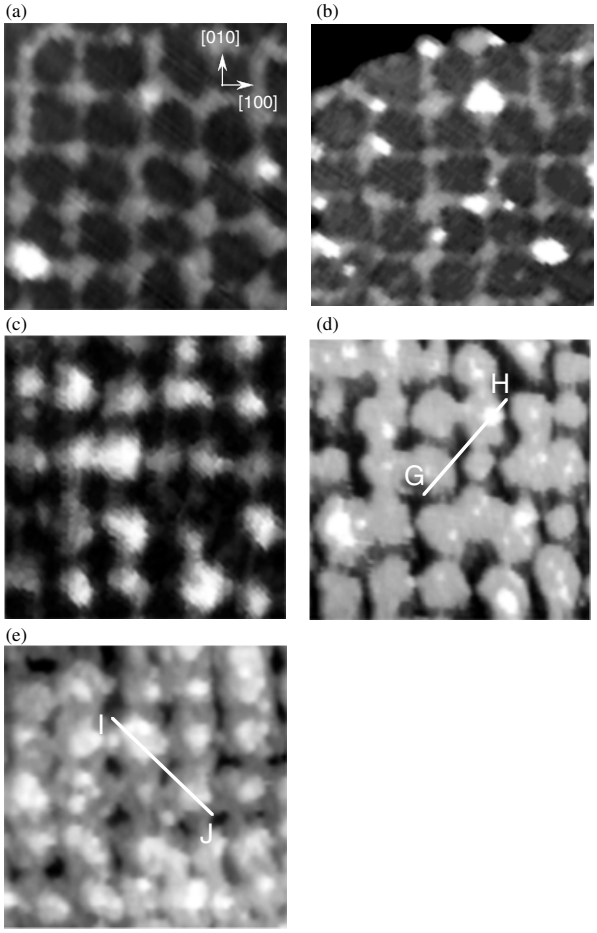

Figure 4. STM images for Fe islands grown on surfaces with squarely arranged c(2 × 2)–N patches. The deposition rate is 0.2 ML min^{-1}, and the averaged thicknesses of Fe are (a) 0.02 ML, (b) 0.05 ML, (c) 0.1 ML, (d) 0.9 ML, and (e) 1.4 ML.

The crystal structure of Fe on clean Cu(001) surface is independent of its width. They claimed that more than 5 ML thick Fe islands are formed selectively on clean Cu surface, keeping c(2 × 2)–N patches free from Fe growth. This is not the case, as shown in the present results by STM observations, when the nitrogen coverage is larger than 0.3 ML. In the previous STM observation by Parker *et al* [14], 4 ML thick Fe islands were formed selectively on the wide Cu line whose width is more than 5 nm. They used the nitrogen-adsorbed surface consisting of wide and narrow clean Cu lines, as in figure 2(b). It is possible that the same surface was used for the SEXAFS experiment.

5.2. Co dot array

Growth of Co on the surface with regular arrangement of the c(2 × 2)–N patches is shown in figure 7. At the initial stage of the deposition, monolayer Co grows selectively on the clean Cu lines, as in figure 7(a), when the line is wider than 1 nm. In contrast to the Fe growth on the Cu grid pattern, there is little selectivity as regards the monolayer Co growth between

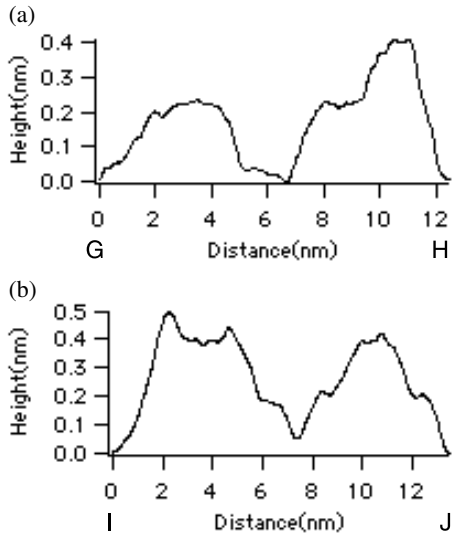

Figure 5. (a) The cross section of the surface along the line G–H in figure 4(d), and (b) that along I–J in figure 4 (e).

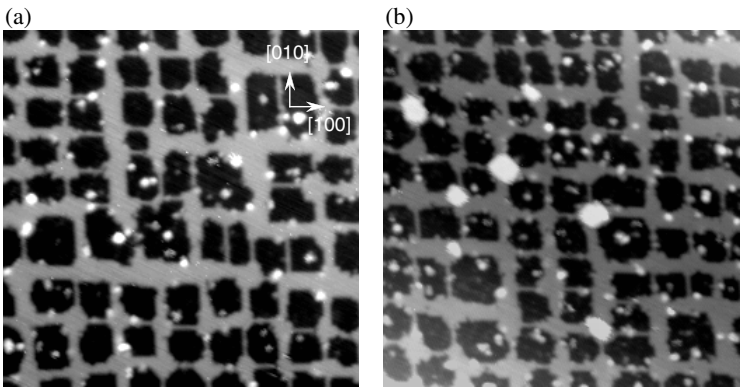

Figure 6. STM images for Fe islands grown on surfaces with squarely arranged c(2 × 2)–N patches. The deposition rate is 2 ML min^{-1}, and the averaged thicknesses of Fe are (a) 0.015 ML, (b) 0.03 ML.

the intersections and the other areas on the clean Cu lines, although there is clear selectivity between the clean Cu surface and the nitrogen-adsorbed surface. With increasing amount of deposited Co on the surface, a monolayer continuous Co grid is formed, and the second layers nucleate selectively at the intersections of that grid, as in figure 7(b). Further deposition of Co results in a square arrangement of the double-layer Co dots interconnected with monolayer Co strips, as shown in figure 7(c). The selective growth of the second-layer Co is similar to the growth of the Fe island growth, whose model is shown in figure 1(b). At this stage, some of the c(2 × 2)–N patches are partly covered with monolayer Co. When the averaged thickness of Co is larger than 1.6 ML, most of the double-layer islands are connected with one another. Furthermore, the third layer is not always formed at the intersections of the clean Cu lines. At the same time, most of the nitrogen-adsorbed patches are mostly covered with monolayer Co

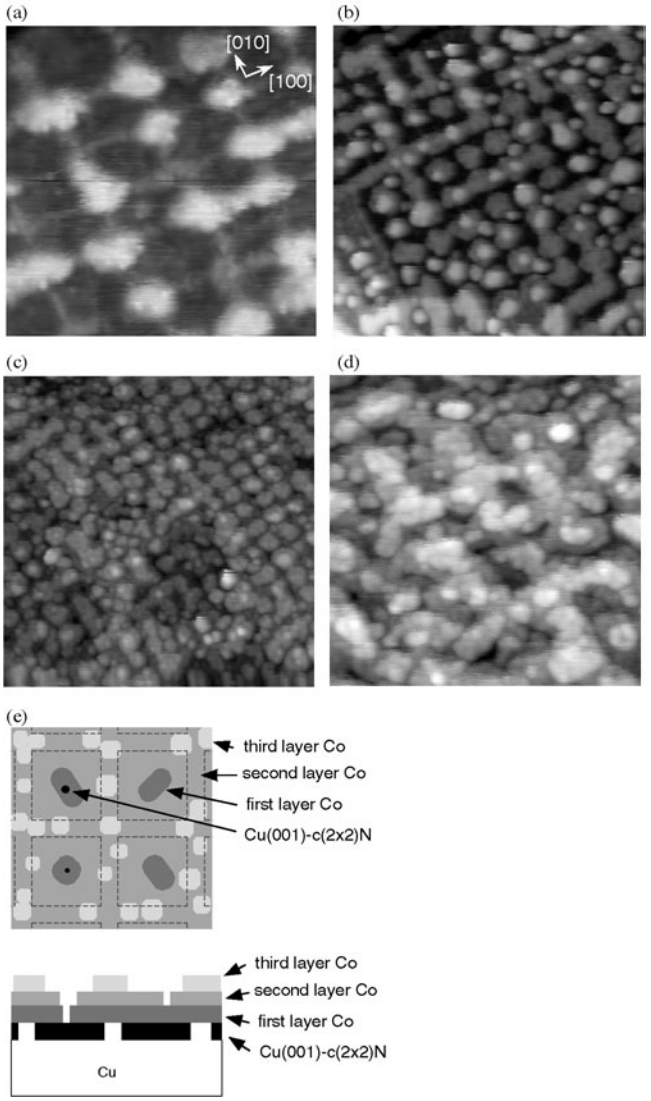

Figure 7. STM images for Co grown on surfaces with squarely arranged c(2 × 2)–N patches ((a)–(d)), and the greyscale schematic illustration (e) for the surface (d). The averaged thicknesses of Co are (a) 0.2 ML, (b) 0.8 ML, (c) 1.4 ML, and (d) 1.9 ML. Dashed lines in (e) indicate the boundaries between the c(2 × 2)–N patches and the clean Cu(001) surfaces.

film at first, and then the second layer is formed on it with an increased average thickness of Co. Consequently, the square arrangement of Co dots becomes disordered. An STM image of such a surface is shown in figure 7(d) for the film with 1.9 ML Co on average. A schematic drawing of the morphology of this film is given in figure 7(e). The c(2 × 2) LEED spots remain for the surfaces with averaged Co coverage of up to 2 ML, as in the case of Fe deposition.

Figure 8 shows an STM image of 200 nm × 200 nm for 1.3 ML Co. We observe a homogeneous arrangement of the Co dots and a distribution of monatomic steps on the substrate. We note that there are at least three kinds of thin Co structure on the surface: monolayer Co on clean Cu lines, monolayer Co on c(2 × 2)–N patches, and double-layer Co dots.

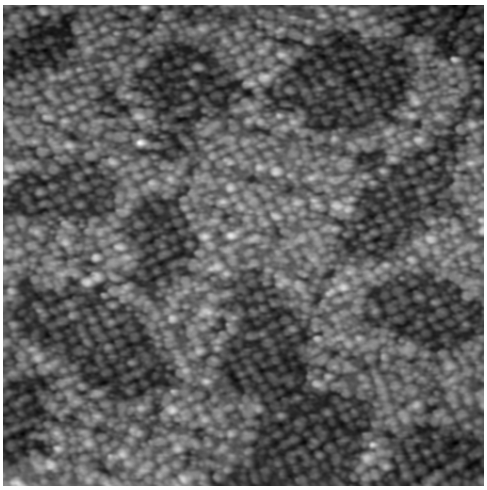

Figure 8. An STM image of squarely arranged double-layer Co dots over a wide area (200 nm × 200 nm) of Cu(001)-c(2 × 2)–N surface with monatomic height steps. The averaged Co thickness is 1.3 ML.

5.3. Selective growth among clean Cu surfaces

When the ferromagnetic transition metals [14, 15, 24–27] are deposited on the square grid pattern of the Cu(001)-c(2 × 2)–N surface at RT, the metal atoms are unreactive to the nitrogen-covered area, and migrate to the clean Cu surface. The c(2 × 2)–N structure is retained with the metal deposition, as confirmed by the fact that the LEED patterns are still c(2 × 2) after the deposition of up to 2 ML metal atoms. At the early stages of the deposition, both Fe and Ni nucleate dominantly at the intersections of the clean Cu lines when their widths are narrower than 3 nm. Even after a very small island nucleates by the increased deposition rate, monolayer dots of a few nanometres in diameter are selectively grown just at the intersections. On the other hand, monolayer Co grows at any place on the clean Cu grid unless the width of the line is narrower than 1 nm.

In the present case, the metal island growth is ruled by a kinetic process of deposited atoms. It consists of their adsorption, migration, and nucleation, or attachment to the nucleation centres. The atoms of magnetic transition metals deposited on the square grid pattern of nitrogen-adsorbed Cu(001) surfaces freely migrate on the c(2 × 2)–N patches without adsorption just after the arrival. Then the very small islands nucleate predominantly on clean Cu surface unless the deposition rate is high enough for the migrating atoms to form nucleation centres before arriving at the clean Cu surface. Thus the observed selective growth of Fe and Ni on clean Cu surface is caused by the difference in either the nucleation site or the growth rate.

To clarify the origin of the selective growth of Fe among clean Cu surfaces on the square grid pattern, we studied the surface with less than 0.01 ML Fe by STM. As shown in figure 9(a), a few dark dots were found on the clean Cu grid in addition to small islands. Here the deposition rate was 2 ML min^{-1}. The apparent depth of the dark dot is 0.1 ML with the tunnelling conditions of −2 V and 0.4 nA.

For the growth of iron thin films on a clean Cu(001) surface, an exchange–nucleation model was proposed by Johnson *et al* [40], as in the case of Fe growth on Au(111) surfaces. They showed that the iron atoms replace the substrate Cu atoms at the initial stages of the deposition. The inclusions of Fe atoms in the Cu surface are imaged as dark dots in STM, as

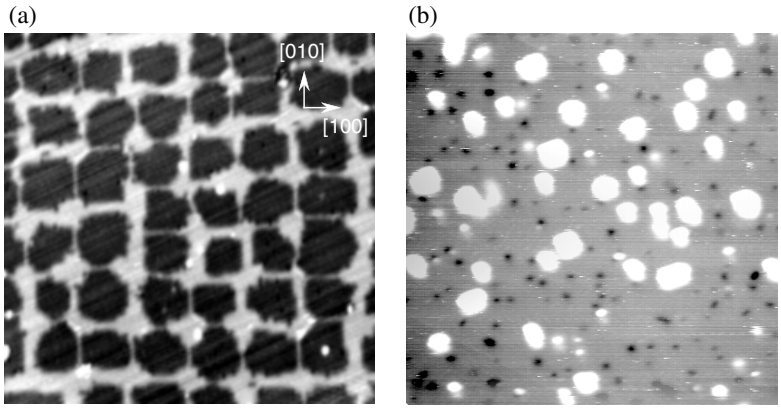

Figure 9. (a) An STM image for Fe deposited on the surface with squarely arranged c(2 × 2)–N patches. The deposition rate is 2 ML min^{-1}, and the averaged thickness of Fe is 0.003 ML. The size of the image is 50 nm × 50 nm. (b) An STM image for Fe deposited on a clean Cu(001) surface. The deposition rate is 2 ML min^{-1}, and the averaged thicknesses of Fe is 0.19 ML. The size of the images is 50 nm × 50 nm.

shown in figure 9(b). This image was obtained after RT deposition of Fe on a clean Cu(001) surface using the tunnelling conditions of 2 V and 0.1 nA. There coexist 0.1 ML deep dots and 1 ML high islands. The former substitutional Fe atoms in the surface are considered [40] to play roles of nucleation centres for the Fe island growth.

The dark dots observed on the square grid pattern are also interpreted as iron inclusions in clean Cu lines. The centre of the intersection is not a position for a dominant inclusion. Instead, we notice the tendency for the Fe-atom inclusions to be formed near to the boundary between the Cu clean surface and the nitrogen-adsorbed patch.

In figure 9(a), the islands whose diameter is smaller than 1 nm do not always distribute at the intersections of the clean Cu grid, and there is no clear selectivity of the island nucleation between the intersection and the other clean Cu surface. They tend to form near the boundary of the nitrogen-adsorbed patches on the clean Cu surface as in the case of Fe inclusions. The same tendency is seen in figure 6(a). This clearly indicates the Fe inclusions are the nuclear centres of the Fe islands.

When we increase amount of Fe deposition, large monolayer islands are formed only at the intersections of the Cu lines, as shown in figure 6(b). This means that the rate of growth from small nucleations to the islands at the intersections is larger than that at the lines and on the nitrogen-adsorbed patches. As discussed in section 4, the surface strain at the centre of the intersection is smaller than in the middle of the line on the grid pattern. The above experimental result indicates that the Fe-atom sticking probability at the side of the small monolayer island depends on the substrate Cu surface strain. It is larger at a less strained surface. Thus, the selective growth of Fe dots at the intersections is caused by the differences in growth rate among the clean Cu surfaces, not by that in the nucleation site.

For the Co deposition, on the other hand, most of the clean Cu surface at the grid is covered by monolayer Co homogeneously. Like in the case of Fe on a clean Cu(001) surface, the atom inclusions in the Cu surface are the nucleation centres for the Co islands on clean surfaces [41, 42]. Thus the nucleation centres of Co islands are expected to distribute randomly on the Cu grid surface as in the case of Fe growth. The experimental results indicate that the rate of growth of the Co islands from their small nucleation centres is independent of the surface strain.

After the monolayer Fe islands cover all the Cu intersections of the grid pattern, the metal atoms stick to their sides, and monolayer islands grow laterally both on clean Cu lines and on c(2 × 2)–N patches. The surface of monolayer Fe islands observed by STM is almost flat and homogeneous, as shown in figure 4(d). It is difficult to distinguish the Fe film on clean Cu surface from that on the c(2 × 2)–N surface. Similar homogeneous STM images were reported for monolayer Co [25, 26] and Ni [15] on the same substrate. The growth of the second layer on the grid pattern for Fe, Co, and Ni commonly occurs at the intersections of the grid pattern where the surface strain is minimum.

There has been discussion on the mixing of Cu in the monolayer Fe and Co islands on clean Cu(001) surfaces. In STM observations [43] for Fe, the exchange was clearly visible when the surface was annealed up to 490 K. On the other hand, at RT, the island mainly consists of Fe. The only evidence of mixing observed is the small difference in apparent height in the STM images, and qualitative studies have not yet been made. For Co grown on clean Cu(001) surface, it was pointed out [41] that the details of the morphology and interface mixing between Co and Cu depend on the deposition rate and the substrate temperature. In the present case, small bumps are found on some of the monolayer Fe islands at the intersections. These can be interpreted as Cu-rich areas, as on the clean Cu surface.

5.4. Growth of Fe and Co on nitrogen-saturated surfaces

On the nitrogen-saturated Cu(001)-c(2 × 2)–N surface, isolated double-layer islands are formed even at the initial stages of Fe deposition [27]. Similar island growth was observed for Co and Ni [15] on this surface, and the growth mode is commonly the Volmer–Weber type. The results are consistent with the growth on the square grid pattern of nitrogen-adsorbed surfaces. The interface interaction of the magnetic transition metals with the nitrogen-adsorbed surface is weaker than that with the clean Cu surface. This causes no wetting layer in their growth.

We notice that the Fe islands tend to be formed in the middle of the terraces, and not near to the trenches and the steps. This trend is common in the island growth of Co and Ni [15] on the same substrate. The result is in contrast to the case of heteroepitaxial growth of metal on metal. In most of the cases, a step is the preferred site for growth of the metal overlayer. The middle of the terrace is the place with the minimum strain on the nitrogen-saturated surface. The selective island growth on less strained areas is similar to the growth on the partly nitrogen-covered Cu(001) grid pattern.

6. Magnetic properties of the Co dot array

We measured the hysteresis curves of the magnetization for Co dot arrays using the SMOKE. Figure 10(a) shows the development of the hysteresis loops measured for the longitudinal configuration at 95 K with increasing averaged Co thickness. In figure 10(b), the magnitude of the remanent magnetization is plotted. The magnetic field is applied in the plane along the [110] direction, which is the easy magnetization axis for the ultrathin Co films grown on a clean Cu(001) surface [33]. The onset of ferromagnetism is apparent from the finite remanence in the hysteresis loops obtained for the 1.3 ML thick film. As the thickness is increased, the magnitude of the magnetization and the coercivity increase. Beyond 2.2 ML the loop exhibits a rectangular shape, implying that the [110] direction is the easy magnetization axis. However, below 2 ML, the loops deviate significantly from this easy axis behaviour. The shapes of the hysteresis loops were almost independent of the sweep rate between 40 and 2.5 Oe s^{-1}. We could not detect any polar SMOKE signal in the Co thickness range investigated. This means that the magnetization is in the plane, just like that in the Co films on a clean Cu(001) surface.

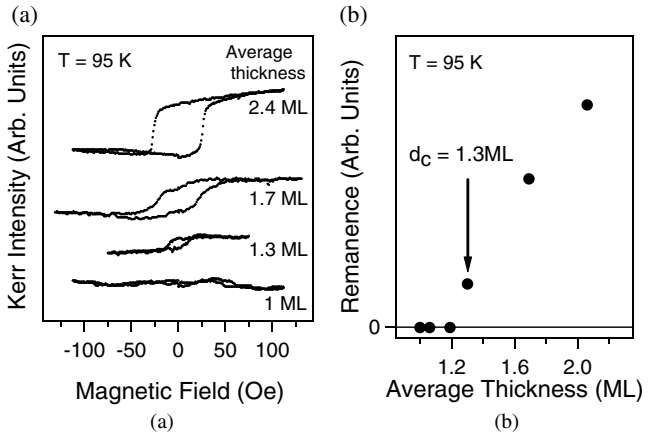

Figure 10. (a) Hysteresis loops of the magnetization along [110] as a function of averaged Co thickness at 95 K. (b) Remanence magnetization at 95 K as a function of averaged Co thickness. An arrow at d_C indicates the critical Co thickness for the appearance of the remanence.

Figure 11 shows the temperature dependence of the hysteresis loops for the averaged Co thicknesses of 1.3 ML (a), 1.6 ML (b), and 1.8 ML (c). We define T_r here as the temperature at which the remanence magnetization vanishes completely. The value of T_r lies around 160 K for 1.3 ML, and 260 K for 1.6 ML. The transition is reversible because the ferromagnetic Kerr loops are reproducible after heat cycling between 90 K and RT. For 1.8 ML, the remanence persists up to 370 K, and T_r is above that temperature. We did not try to measure the Kerr loops over 400 K because the significant intermixing of Co with Cu may change the magnetic properties [32].

In figure 12, we show the remanent magnetization as a function of temperature for 1.6 and 1.8 ML. The remanence increases below 150 K with decreasing temperature for the 1.8 ML Co film, in which the saturated magnetization also increases below this temperature. Similar increases of the magnetization were observed for 1.9 and 2.1 ML.

The change of T_r is plotted in figure 13 as a function of Co thickness. The uncertainty in the Co thickness is shown at the point for 1.3 ML. The arrows pointing up and down for 1.2 and 1.9 ML mean that the corresponding T_r is below 100 K and above 400 K, respectively. For comparison, the values of T_C for ultrathin Co films grown on clean Cu(001) surfaces [33, 44] are reproduced as dashed and solid lines. We note that the definition of T_C for the Co films on clean Cu(001) is experimentally the same as that of T_r for the present system.

The measured T_r for Co on Cu(001)-c(2 × 2)–N is found to be higher than T_C for Co/Cu(001) with the same nominal thickness within our experimental accuracy. This is ascribed to the difference in growth morphology of the Co islands. On the Cu(001)-c(2 × 2)–N surface, double-layer islands are connected with one another and the third layer is formed with an increased average thickness of Co. Even after the growth of the third layer, there remain small areas of bare c(2 × 2)–N surface at the centre of the patches. On the other hand, on clean Cu(001) surfaces, Co films are known to grow as double-layer islands just before coalescence [41]. Consequently, the percolative transition [6] to a long-range ferromagnetic state for double-layer Co dots on Cu(001)-c(2 × 2)–N should occur even if the averaged thickness of Co is smaller than that of the Co film on clean Cu(001). The increase of the effective thickness due to the confined growth of Co islands on Cu(001)-c(2 × 2)–N causes T_r to be higher than T_C for the Co films on clean Cu(001).

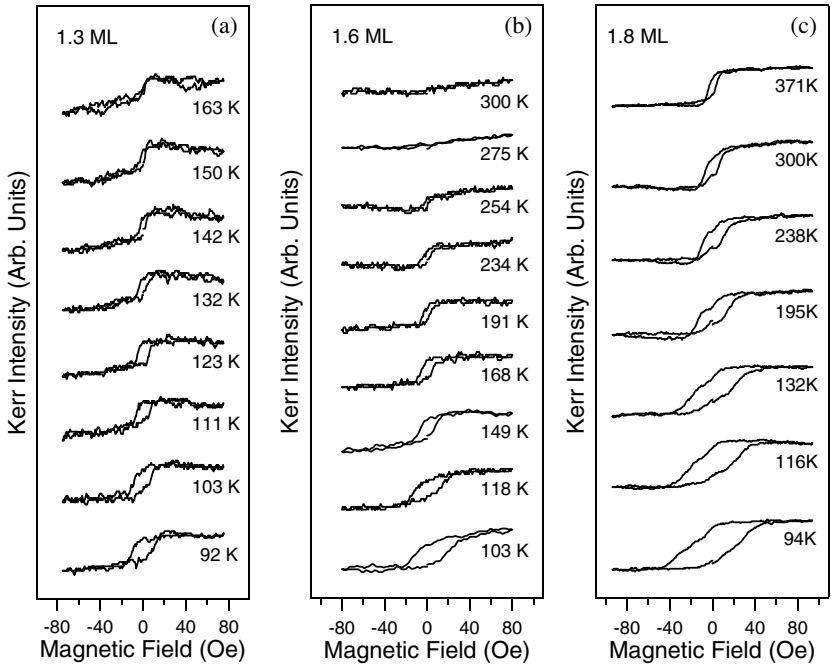

Figure 11. Hysteresis loops as a function of temperature for three samples. The averaged thicknesses of Co are (a) 1.3 ML, (b) 1.6 ML, and (c) 1.8 ML.

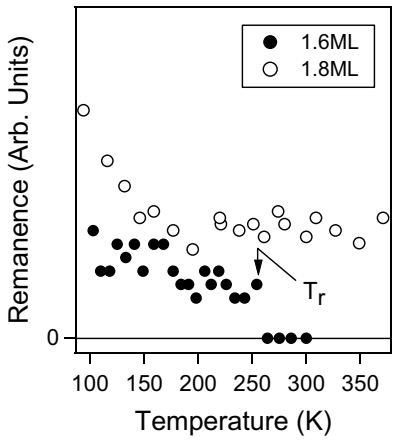

Figure 12. Remanence magnetization as a function of temperature for the samples with 1.6 ML (closed circles) and 1.8 ML (open circles) Co on average. The transition temperature T_r of the 1.6 ML thick sample is indicted by an arrow.

For an averaged thickness of <1.4 ML, the double-layer Co dots are separated from one another although they are connected with short monolayer strips of Co, as schematically illustrated in figure 1(b). These double-layer dots do not seem to interact directly via exchange interaction, because the monolayer Co on clean Cu(001) surface is not ferromagnetic down to 50 K [33, 44]. Thus, the array of isolated double-layer Co dots is expected to exhibit a superparamagnetic behaviour below the Curie temperature for 2 ML thick Co films on a clean

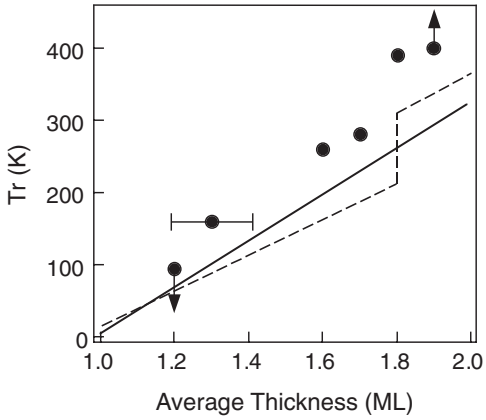

Figure 13. The transition temperature T_r as a function of the averaged thickness of Co. Solid and dashed lines show the Curie temperature T_C for Co films on clean Cu(001) surfaces reproduced from [33] and [44] respectively.

Cu(001) surface. Each double-layer Co dot has a spontaneous magnetization, and its direction is thermally fluctuating above the blocking temperature. The magnetization curves characteristic of the superparamagnetism are really observed at 1.3 ML above 160 K and at 1.6 ML above 260 K (figures 11(a), (b)) with no remanence but finite magnetization in a magnetic field.

The presence of remanence below 150 K for the 1.3 ML film suggests the transition from the array of superparamagnetic Co dots to a long-range ordered 2D ferromagnet. Generally, the long-range order can be established among superparamagnetic nanodots at a certain low temperature through inter-dot magnetic coupling. In our films, superparamagnetism of each double-layer Co dot is ensured by exchange interaction among the Co atoms in the dot, whereas the inter-dot magnetic coupling is mediated by the short strips of monolayer Co. It is possible that each double-layer Co island has a sufficient magnetic moment to polarize nearby Co atoms, mediating exchange interaction in the monolayer strips.

Below 1.2 ML, the magnetic interaction mediated by the short Co strips is too weak to induce long-range ferromagnetism above 95 K, although each double-layer Co dot may behave as a superparamagnet. For these films, we could not detect any evidence of superparamagnetism, which should be examined by using higher magnetic fields, as demonstrated for Co dots on Au(111) surfaces [20]. The maximum magnetic field of 200 Oe in the present study is insufficient to saturate all the superparamagnetic moments at the Co dots even at 95 K.

Another possible explanation of the hysteresis loop at 1.3 ML below 150 K in the present system is the blocking of superparamagnets as in the case of Co dots on Au(111) surfaces [19]. The blocking generally occurs with decreasing temperature when the relaxation time of the superparamagnet, τ, becomes longer than the measurement time. We observed that the hysteresis curve is independent of the sweep rate if it is faster than 2.5 Oe s^{-1}. This experimentally excludes the blocking as long as τ is shorter than a few minutes.

The value of τ at T for a particle with a volume V can be estimated from the Néel equation [45] given by

$$\frac{1}{\tau} = f_0 \exp \frac{-KV}{k_B T}, \tag{1}$$

where K is the absolute value of the intrinsic magnetic anisotropy constant and f_0 the characteristic frequency of the magnetic system, of the order of 10^9. Using this equation

with the known anisotropic constant of Co film on clean Cu(001), $K = 10^6$ erg cm^{-3} [46], and $T = 150$ K, we obtain $\tau = 10^{-19}$ s for a double-layer island 5 nm $\times$ 5 nm in lateral size. This is much shorter than the measurement time, and it is hard to see how one can attribute the remanence magnetization to the blocking. In the case of Co nanodots on Au(111) surfaces [19], the value of K is enhanced and blocking of the superparamagnetism is observed. On the Au(111) surface, however, both the magnetic anisotropy and the effective volume become large, because one-dimensional short clusters made of several Co nanodots form [20].

We observed changes of the hysteresis loop of the magnetization below 150 K—that is, increasing remanence and saturation magnetization—for the Co films with thickness between 1.8 and 2.1 ML, as in figures 11 and 12. In these films, 2 or 3 ML thick Co dots are connected well with one another, and T_r is higher than 370 K. The magnetization due to the double-layer or triple-layer Co films on these surfaces should be saturated below 150 K, which is much less than their temperature of transition to the long-range ferromagnetic state. Consequently, the origin of the increasing magnetization with decreasing temperature below 150 K is sought in the monolayer Co films on the c(2 $\times$ 2)–N patches. As shown in figure 7(e) schematically, they are at the centres of the patches. The polarization in the monolayer area may be induced by the surrounding double- or triple-layer Co films. It is even possible that the monolayer Co has a spontaneous magnetization at low temperature. The Co film on the c(2 $\times$ 2)–N patch is free from mixing with Cu, and could be an ideal system to compare with the theoretically predicted magnetic polarization of monolayer Co.

For the 1.6 ML thick film, the remanence magnetization due to the double-layer dots gradually increases with decreasing temperature from $T_r = 260$ K, and has no clear plateau. Thus, we could not experimentally separate the induced polarization at the monolayer area from the magnetization due to the double-layer dots. For the film with more than 2.2 ML thick Co, the area with monolayer Co becomes very small, and the magnetic properties become almost the same as for the Co film on a clean Cu(001) surface.

Reduced remanence from the saturated magnetization was observed for the films with averaged thickness <2.1 ML. This implies possible change of the easy magnetization axis along ⟨110⟩ [33] for the fcc Co film on a clean Cu(001) surface. There are three sources of magnetic anisotropy: the magnetocrystalline anisotropy, the shape anisotropy, and the anisotropy due to the presence of steps. If Co on the nitrogen-modified Cu(001) grows as fcc Fe on the same substrate [39], the magnetocrystalline anisotropy is the same as that for a Co film on clean Cu(001). The recovery of full remanence beyond 2.2 ML supports the fcc structure of Co. This favours anisotropy along ⟨110⟩. Since the Co strips on the Cu(001)-c(2 $\times$ 2)–N are along the ⟨100⟩ direction, the shape anisotropy favours the ⟨100⟩ direction as an easy magnetization axis. The measurement of Kerr loops along the [100] direction, however, did not produce rectangular shapes. This indicates that the shape anisotropy imposed by the arrangement of Co dots is not a dominant factor in determining the easy axis. The presence of steps on the substrate has a profound influence on the magnetic anisotropy [47, 48]. The step density on the substrate increases after the formation of regularly arranged square patches of c(2 $\times$ 2)–N islands is shown in figure 2(d). In the STM images, steps run along both the ⟨110⟩ and ⟨100⟩ directions, although the former slightly dominates over the latter. Therefore, the three sources of anisotropy compete with one another, and easy magnetization axis behaviour is not clearly observed in the present system.

7. Summary and outlook

We have demonstrated the formation of Fe and Co nanometre-scale dots arranged squarely on a Cu(001)-c(2 $\times$ 2)–N surface. At the initial stages of the deposition, the atoms selectively

cover the clean Cu area on the surface, consisting of squarely ordered c(2 × 2)–N patches and clean Cu grids a few nanometres in width. In the case of Fe growth, small islands are homogeneously nucleate on the clean Cu surface first, and then lattice points of the Cu grid are dominantly covered with monolayer Fe owing to the high rate of island growth at these positions. The inclusions of Fe atoms in the clean Cu lines of the grid pattern play the roles of the nucleation centres, as in the growth of Fe films on clean Cu(001) surfaces. Double-layer Fe dots are formed selectively at the intersections of the Cu grid after most of the clean Cu surface is covered with monolayer Fe. The double-layer Co dot array is formed in a similar way, while the growth rate of monolayer Co is homogeneous over the clean Cu surface.

In the Co dot arrays, the temperature of the transition between a paramagnetic state and a long-range 2D ferromagnetic state increases with increasing average Co thickness, and is higher than that for a Co film directly deposited on a clean Cu(001) surface with the same average thickness. This is attributed to the confined growth of Co islands on the grid pattern. Remanent magnetization is observed for the 1.3 ML film in which the double-layer Co dots are connected through short Co monolayer strips. For the films with averaged thickness between 1.8 and 2.1 ML, the magnetization increases with decreasing temperature below 150 K, which is much smaller than the corresponding temperature of the transition to the long-range ferromagnetic state. Considering all of these results, we propose that the polarization is induced in the monolayer Co films by the neighbouring double-layer Co dots for 1.8-2.1 ML films, and that the short Co monolayer strips mediate the ferromagnetic interaction among the isolated double-layer Co dots in the 1.3 ML film.

Further detailed microscopic and spectroscopic studies are, however, needed to understand the magnetism of a few-monolayers thick dots, and their assembly. The magnetic study will also have to be extended to dot arrays made of various magnetic metals and alloys. For example, an out-of-plane easy magnetization axis is expected for the Fe dot array. For the industrial application of ultrahigh-density recording, nanomagnets with strong magnetic anisotropy are desirable to overcome the superparamagnetic behaviour of small magnets. This will be achieved by selecting suitable combinations of metals. The use of the strain-relief patterns is not restricted to the fabrication of magnetic nanodots. Selective adsorption and growth of other functional materials, such as catalytic metals, semiconductors, and organic molecules, are promising applications. In these cases also, the grid pattern of the nitrogen-adsorbed Cu(001) surface will provide a useful template.

Acknowledgments

We would like to thank K Tanaka, Y Matsumoto, M Yamada and K Mukai for valuable discussions on the growth of the dot array, K-D Lee, T Iimori, Y Q Cai and K Hattori for collaboration and discussions on the study of magnetism. This work was supported by Core Research for Evolutional Science and Technology, Japan Science and Technology Corporation.

References

[1] Bland J A C and Heinrich B (ed) 1994 *Ultrathin Magnetic Structures I* (Berlin: Springer)
[2] Heinrich B and Bland J A C (ed) 1994 *Ultrathin Magnetic Structures II* (Berlin: Springer)
[3] Himpsel F J, Ortega J E, Mankey G J and Willis R F 1998 *Adv. Phys.* **47** 511
[4] Billas I M L, Chatelain A and de Heer W A 1997 *J. Magn. Magn. Mater.* **168** 64
[5] Elmers H J, Hauschild J, Höche H, Gradmann U, Bethge H, Heuer D and Koehler U 1994 *Phys. Rev. Lett.* **73** 898
[6] Schumann F O, Buckley M E and Bland J A C 1994 *Phys. Rev.* B **50** 16 424

[7] Pedersen M Ø, Bönicke I A, Lægsgaard E, Stensgaard I, Rubion A, Nørskov J K and Besenbacher F 1997 *Surf. Sci.* **387** 86
[8] Shen J, Klaua M, Ohresser P, Jenniches H, Barthel J, Mohan Ch V and Kirschner J 1997 *Phys. Rev.* B **56** 11 134
[9] Gu E, Hope S, Tseleip M and Bland J A C 1999 *Phys. Rev.* B **60** 4092
[10] Hauschild J, Elmers H J and Gradmann U 1998 *Phys. Rev.* B **57** 677
[11] Shen J, Skomski R, Klaua M, Jenniches H, Sundar S, Manoharan S S and Kirschner J 1997 *Phys. Rev.* B **56** 2340
[12] Chambliss D D, Wilson R J and Chiang S 1991 *Phys. Rev. Lett.* **66** 1721
[13] Voigtländer B, Meyer G and Amer N M 1991 *Phys. Rev.* B **44** 10 354
[14] Parker T M, Wilson L K, Condon N G and Leibsle F M 1997 *Phys. Rev.* B **56** 6458
[15] Matsumoto Y and Tanaka K 1998 *Japan. J. Appl. Phys.* **37** L154
[16] Brune H, Giovannini M, Bromann K and Kern K 1998 *Nature* **394** 451
[17] Meyer J A, Baikie I D, Kopatzki E and Behm R J 1996 *Surf. Sci.* **365** L647
[18] Dovek M M, Lang C A, Nogami J and Quate D F 1989 *Phys. Rev.* B **40** 11 973
[19] Dürr H A, Dhesi S S, Dudzik E, Knabben D, van der Laan G, Goedkoop J B and Hillebrecht F U 1999 *Phys. Rev.* B **59** 701
[20] Padovani S, Chado I, Scheurer F and Bucher J P 1999 *Phys. Rev.* B **59** 11 887
[21] Lee R N and Fansworth H E 1965 *Surf. Sci.* **3** 461
[22] Leibsle F M, Flipse C F J and Robinson A W 1993 *Phys. Rev.* B **47** 15 865
[23] Leibsle F M, Dhesi S S, Barret S D and Robinson A W 1994 *Surf. Sci.* **317** 309
[24] Mukai K, Matsumoto Y, Tanaka K and Komori F 2000 *Surf. Sci.* **450** 44
[25] Silva S L, Jenkins C R, York S M and Leibsle F M 2000 *Appl. Phys. Lett.* **76** 1128
[26] Komori F, Lee K D, Nakatsuji K, Iimori T and Cai Y Q 2001 *Phys. Rev.* B **63** 214420
[27] Ohno S, Nakatsuji K and Komori F 2001 *Surf. Sci.* **493** 539
[28] Silva S L and Leibsle F M 1999 *Surf. Sci.* **440** L835
[29] Lee K D, Iimori T and Komori F 2000 *Surf. Sci.* **454–6** 860
[30] Sotto M, Gauthier S, Pourmir F, Rousset S and Klein J 1997 *Surf. Sci.* **371** 36
[31] Sotto M and Croset B 2000 *Surf. Sci.* **461** 78
[32] Schmid A K, Atlan D, Ito H, Heinrich B, Ichinokawa T and Kirschner J 1993 *Phys. Rev.* B **48** 2855
[33] Schneider C M, Bressler P, Schuster P, Kirschner J, de Miguel J J and Miranda R 1990 *Phys. Rev. Lett.* **64** 1059
[34] Ellmer H, Repain V, Rousset S, Croset B, Sotto M and Zepenfeld P 2001 *Surf. Sci.* **476** 95
[35] Hoeft J T, Polick M, Kittel M, Terborg R, Toomes R L, Kang J-H and Woodruff D P 2001 *Surf. Sci.* **492** 1
[36] Driver S M and Woodruff D P 2001 *Surf. Sci.* **492** 11
[37] Yoshimoto Y and Tsuneyuki S 2002 *Surf. Sci.* at press
[38] Cohen C, Ellmer H, Guigner J M, L'Hoir A, Prevot G, Schmaus D and Sotto M 2001 *Surf. Sci.* **490** 336
[39] D'Addato S, Binns C and Finetti P 1999 *Surf. Sci.* **442** 74
[40] Johnson K E, Chambliss D D, Wilson R J and Chiang S 1993 *J. Vac. Sci. Technol.* A **11** 1654
[41] Fassbender J, Allenspach R and Dürig U 1997 *Surf. Sci.* **383** L742
[42] Nouvertne F, May U, Bamming M, Rampe A, Korte U, Guntherodt G, Pentcheva R and Scheffler M 1999 *Phys. Rev.* B **60** 14 382
[43] Shen J, Giergiel J, Schmid A K and Kirschner J 1995 *Surf. Sci.* **328** 32
[44] Bovensiepen U, Poulopoulos P, Platow W, Farle M and Baberschke K 1999 *J. Magn. Magn. Mater.* **192** L386
[45] Néel L 1949 *Ann. Geophys.* **5** 99
[46] Heinrich B, Cochran J F, Kowalewski M, Kirschner J, Celinski Z, Arrott A S and Myrtle K 1991 *Phys. Rev.* B **44** 9348
[47] Berger A, Linke U and Oepen H P 1992 *Phys. Rev. Lett.* **68** 839
[48] Kawakami R K, Bowen R O, Choi H J, Escorcia-Aparicio E J and Qiu Z Q 1998 *Phys. Rev.* B **58** 5924